J Fluoresc (2017) 27:205–211
DOI 10.1007/s10895-016-1947-4

ORIGINAL ARTICLE

A Novel Fluorescent Biosensor for Detection of Silver Ions Based on Upconversion Nanoparticles

Qian Long[1] · **Yanqing Wen**[1] · **Haitao Li**[1] · **Youyu Zhang**[2] · **Shouzhuo Yao**[2]

Received: 16 July 2016 / Accepted: 3 October 2016 / Published online: 22 October 2016

Abstract In this paper, we report a simple and sensitive fluorescent biosensor for the quantitative analysis of silver ions (Ag^+) by using $NaYF_4$:Yb^{3+}, Tm^{3+} upconversion nanoparticles (UCNPs). Ag^+ could oxidize o-phenylenediamine (OPD) to the oxidized OPD (oxOPD) directly. The fluorescence of UCNPs can be significantly quenched by oxOPD through inner filter effects (IFE). Under the optimized conditions, the Ag^+ concentration is proportional to the changes of the fluorescence intensity of UCNPs. The proposed method shows high selectivity and Ag^+ could be quantitatively detected in the range of 0 to 0.5 mM with a low detection limit of 33 nM for Ag^+. The selectivity and sensitivity of the detection can also be satisfactory. More importantly, this method has potential in practical application to detect Ag^+ in real samples without interference.

Keywords Upconversion nanoparticles · Ag^+ · O-phenylenediamine · Inner filter effects

Electronic supplementary material The online version of this article (doi:10.1007/s10895-016-1947-4) contains supplementary material, which is available to authorized users.

✉ Youyu Zhang
zhangyy@hunnu.edu.cn

[1] Hunan Vocational Institute of Safety Technology, Changsha 410151, China

[2] Key Laboratory of Chemical Biology and Traditional Chinese Medicine Research (Ministry of Education),College of Chemistry and Chemical Engineering, Hunan Normal University, Changsha 410081, China

Introduction

Silver ions (Ag^+) is widely used in the electrical industry, photography imaging industry and pharmacy [1–3]. It has been considered to be a high-effect fungicide for a long time, which is always thought to be a precious metal safe to humans [4]. The standard safe concentration of Ag^+ for human is <0.05 ppm according to the World Health Organization (WHO) [5]. But thousands of tons of Ag^+ are released to the environment from industrial wastes and emissions annually. Excessive amounts of Ag^+ are distributed and contaminated in ambient air, water, and soil, which may lead to serious environmental problems [6, 7]. And it can accumulate in human body through the food chain, and causing various problems to the human health such as cytotoxicity, organ failure, and reduction in mitochondrial function [4, 8]. Therefore, it has received considerable attention in recent years and recent studies emphasized bioaccumulation and the potential negative impact of Ag^+ [9]. Hence, the quantitative determination of Ag^+ is of great significance in diagnosing related diseases.

Nowadays, several technologies have been developed for Ag^+ detection, including atomic absorption/emission spectroscopy [10–13], inductively coupled plasma-mass spectroscopy [14, 15], ion-selective electrodes (ISEs) [16, 17], voltammetry [18–20], ultraviolet–visible (UV–vis) [6, 21], florescence method [3, 22, 23] and electrochemical chemosensing [4, 5]. Despite tremendous efforts being made in detection of Ag^+ with high selectivity and sensitivity, all these abovementioned methods suffer from more or less drawbacks such as sophisticated equipment, complicated sample preparation processes, high cost, relatively high temperature and time-consuming immobilizing processes, which limit their wide application. Compared to other choices, the florescence methods in detection of Ag^+ are fast, efficient and sensitive. Recently, the method that visual and trap emission

spectrometric detections of Ag^+ with mesoporous ZnO/CdS@SiO_2core/shell nanocomposites has been developed [1]. However, it is difficult to eliminate the background interference resulted from the detection systems, which affects the sensitivity and detection limit. Therefore, it is essential to monitor Ag^+ without background interference through fluorescence methods.

In recent years, increasing attention has been paid to the upconversion nanoparticles (UCNPs) and their potential applications [24–31]. UCNPs doped with certain rare earth ions which the low energy near-infrared light (typical 980 nm) can be converted into a higher energy visible emission via a two-photon or multiphoton mechanism [32–34]. Comparing with conventional fluorescent labels, as fluorescent biolabels, UCNPs possess several outstanding features including narrow emission peaks, large Stokes shifts, low toxicity, high photostability and thermal stability, minimum photodamage to living organisms, no autofluorescence and high signal-to-noise ratio [24, 35]. Thus, these excellent fluorescence properties make the UCNPs exploited to develop biosensors for a wide variety of target analytes.

In this study, enlightened by the above facts, we have developed a new UCNPs-based optical biosensor for Ag^+ determination. The proposed detection strategy was shown in Scheme 1. Ag^+ can oxidize o-phenylenediamine (OPD) to induce a yellow color and an absorption peak centered at 450 nm. The fluorescence of UCNPs can be significantly quenched by oxOPD through inner filter effects (IFE), which was proportional to Ag^+. The high selective and sensitive detection of Ag^+ was possible using the fluorescent method. Furthermore, this method has been successfully applied to the determination of Ag^+ in real samples.

Experimental

Materials

Rare earth oxides, including Y_2O_3, Yb_2O_3, Tm_2O_3, were purchased from china national pharmaceutical group corporation (Shanghai, China). $AgNO_3$, $CaCl_2$, $CdCl_2$, $CoCl_2$, $CuCl_2$, $FeCl_3$, $Hg(NO_3)_2$, $Mg(OAc)_2$, $MnCl_2$, $NiCl_2$, $PbCl_2$, $ZnCl_2$ and $FeCl_2$ were purchased from Beijing Chemical Corp. All the other chemicals (99 %, Merck) used in this work were of analytical grade and Millipore Milli-Q ultrapure water was used throughout the experiments.

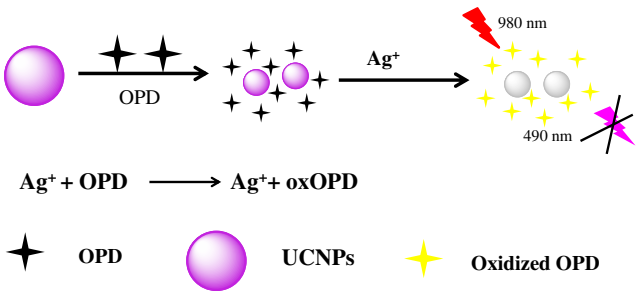

Scheme 1 Schematic illustration of the UCNPs fluorescence assay for the detection of Ag^+

Apparatus

The UV-2450 spectrophotometer (Shimadzu Co., Japan) was used to collect the absorption spectra of oxOPD. The fluorescent emission spectra of UCNPs were recorded by the F-4500 fluorescence spectrophotometer (Hitachi Co., Japan). Transmission electron microscopy (TEM) images were collected by the JEOL-1230 transmission electron microscope (JEM-3010 Joel, Japan). Fourier transform infrared (FTIR) spectra were collected on a Nicolet Nexus 670 FTIR spectrometer (Nicolet Instrument Co., U.S.A.).

Preparation of UCNPs

PEI-modied water-soluble $NaYF_4$:Yb^{3+}, Tm^{3+} were synthesized via a solvothermal method according to the previously reported method [36]. NaCl (0.15 g), PEI (0.4 g), $Y(NO_3)_3$ (0.4 mmol, 0.295 mL), $Yb(NO_3)_3$ (0.20 mmol, 0.6 mL), and $Tm(NO_3)_3$ (0.05 mmol, 0.04 mL) were dissolved in ethylene glycol (15 mL) under vigorous stirring. When the solution became transparent, NH_4F (4 mmol) in EG (10 mL) was added to it. After being stirred for another 10 min, the mixture was transferred into a teflon-lined autoclave and heated to 200 °C for 4 h. Then, the solution was cooled down to room temperature naturally. The nanocrystals were precipitated from the solution by centrifugation and washed sequentially three times by using deionized water and ethanol. The product was dried in vacuum before it was used.

Assay for Ag^+ in Aqueous Buffer

The detection procedure of Ag^+: various amounts of Ag^+ were added to same OPD (1 mM), UCNPs (50 μL, 0.1 mg mL^{-1}), citrate buffer (100 mM, pH = 5.0), which were then kept for 10 min at 30 °C. The fluorescence emission spectra were measured with excitation wavelength at 980 nm. The relationships between the fluorescence intensity and the concentrations of Ag^+ were plotted into calibration curves.

Detection of Ag^+ in Real Samples

The proposed method applied to detect Ag^+ was applied for the direct analysis of Ag^+ in tap water to verify feasibility of this new Ag^+ probe. 100 mL tape water was mixed with Ag^+ aqueous solution, OPD (1 mM), and UCNPs (0.1 mg mL^{-1}). Then citrate buffer (100 mM, pH = 5.0) was added into mixed solution and made up the final volume of 500 mL. And then

the fluorescence emission spectra were measured with excitation wavelength at 980 nm.

Results and Discussion

Characterization of the UCNPs

The morphology, structure, and optical properties of UCNPs were characterized firstly (Fig 1). As shown in Fig. 1a, the TEM images of UCNPs are uniform in morphology with the average sizes of 40 nm. The typical XRD patterns of the UCNPs are presented in Fig. 1b. $NaYF_4$:Yb, Tm nanocrystals were obtained consisting of a dominant cubic phase (JCPDS no.77–2042) by the XRD pattern, indicating that the highly crystalline nature possessed the synthesized material. FT-IR spectra were used to analyze the functional groups on the surface of UCNPs. As shown in Fig. 1c, the methylene asymmetric and symmetric C − H stretching (2960, 2850 cm^{-1}), N − H stretching vibration (3441 cm^{-1}), amine N − H bending (1640 cm^{-1}), and amide bonds internal vibration (1380 cm^{-1}) were correspond to the characteristic peak of amine groups ($-NH_2$), which exhibited characteristic absorption peaks of PEI molecules (Fig. S1). Figure 1d shows the upconversion fluorescence spectrum of the aqueous dispersion under 980 nm laser excitation, a characteristic peak at 490 nm observed. Upon further investigation, we found that the fluorescence intensity of UCNPs possessed excellent photostability over 60 min in air (Fig. S2A) and was not affected by temperature (Fig. S2B) and the pH (Fig. S2C).

The Principle for Detection of Ag^+

The detection mechanism is based on the facts that the fluorescence of UCNPs can be significantly quenched by oxOPD. OPD could be oxidized by Ag^+ and the fluorescence of UCNPs can be quenched by oxOPD. As shown in Fig. 2, UCNPs solution exhibits a maximum fluorescent signal at 490 nm (1). Compared to other signal source, UCNPs has been broadly applied in biosensor because it generates visible emission with low-energy NIR excitation (normally 980 nm). UCNPs could eliminate the autofluorescence from biological macromolecules and thus provides an enlarged signal-to-background ratio and increased sensitivities. The fluorescence of UCNPs was quenched when UCNPs was mixed with Ag^+/OPD system (4, 5, 6). In order to evaluate the feasibility of this assay for Ag^+, we investigated the effects of the related factors. As shown in Fig. 2, the fluorescent intensity of UCNPs has no significant change when UCNPs individually incubated with OPD and $AgNO_3$ under the same conditions (2, 3). The results indicated that the factors mentioned above should not affect the experimental results and OPD plays an important role in the quenching effect of the system.

In this work, the possible mechanism for UCNPs capped PEI quenching was related to inner filter effects (IFE) or fluorescence resonance energy transfer (FRET). It has been reported that the absorption of the excitation and/or emission light by absorbers may reduce the FL intensity of the fluorophore; i.e., FL can be quenched by the so-called inner filter effect [37–39]. The UV–vis absorption spectroscopy and fluorescence emission spectra were measured to study the mechanism. UV-vis absorptions pectroscopy of oxOPD solution in

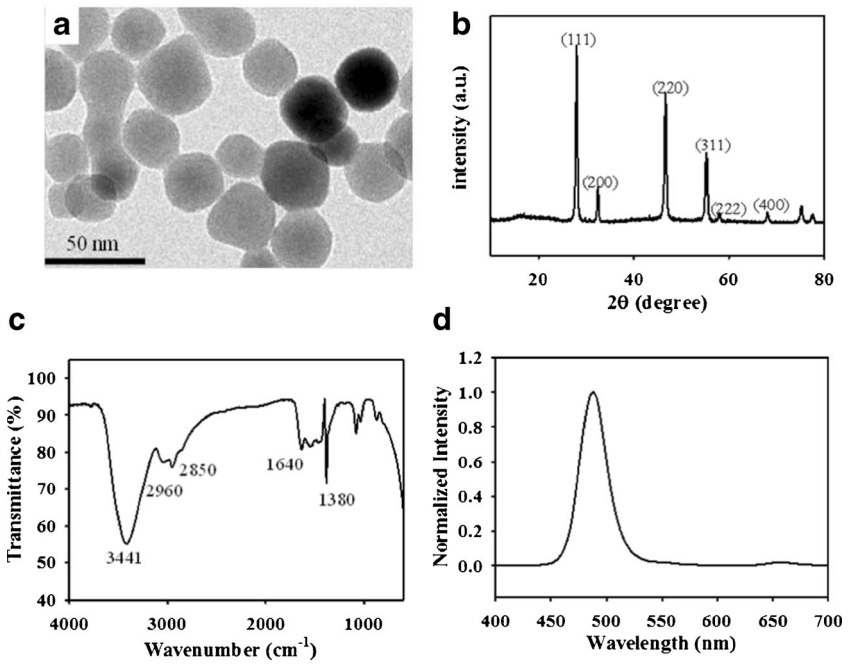

Fig. 1 (**a**) TEM images of the as-prepared water-soluble PEI-$NaYF_4$:Yb,Tm UCNPs. (**b**) XRD patterns of the $NaYF_4$:Yb,Tm UCNPs. (**c**) FTIR spectra of the $NaYF_4$:Yb,Tm UCNPs. (**d**) Emission spectrum of $NaYF_4$:Yb,Tm UCNPs

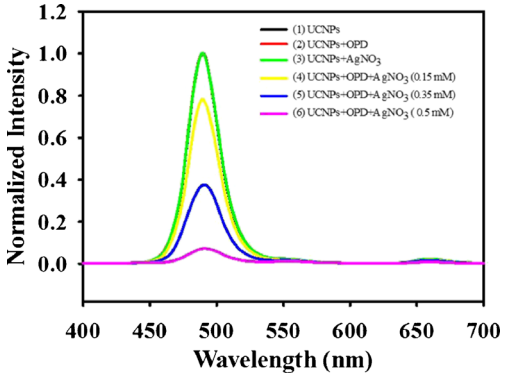

Fig. 2 Fluorescence spectra of UCNPs solution. (1) only UCNPs, (2) UCNPs + OPD, (3) UCNPs + $AgNO_3$, (4) UCNPs + OPD + $AgNO_3$ (0.15 mM), (5) UCNPs + OPD + $AgNO_3$ (0.35 mM), (6) UCNPs + OPD + $AgNO_3$ (0.5 mM), respectively. [UCNPs]: 0.1 mg/mL. [OPD]: 1 mM

the absence and presence UCNPs were recorded (Fig. S3(4,5)). No change in the absorption bands position and absorption intensity of oxOPD was observed after adding UCNPs, which indicated that no complex was formed and fluorescence resonance energy transfer (FRET) between oxOPD and UCNPs does not occur. From the absorption spectrum of oxOPD (Fig. S3(4)), we found that the aqueous pink solution of oxOPD displayed intense absorption at 450 nm. The water-soluble UCNPs were prepared through aqueous-phase synthesis, and they showed a fluorescence emission maximum at 490 nm (Fig. S3(6)), which overlapped very well with the absorption spectrum of oxOPD to induce IFE between them [39–41]. Simultaneously, we investigated the effects of the related factors. As shown in Fig. S3, the absorption intensity of them has no significant change when UCNPs individually incubated with OPD and $AgNO_3$ under the same conditions (1–3). The results indicated that the factors mentioned above should not affect the experimental results. For further confirmation, the zeta potential was then measured to examine the change of surface charges in buffer solution and the experimental results showed the zeta potentials of dispersed UCNPs and oxOPD were all negative. Because both UCNPs and oxOPD are negatively charged, oxOPD could not be adsorbed on the surface of UCNPs via electrostatic interaction and their distanc should be greater than 10 nm. Therefore, the FRET between UCNPs and oxOPD can not occur in buffer solution. Judging from the above analysis, it is obvious that IFE contributed to the observed fluorescence decrease of UCNPs in the presence of oxOPD.

Optimization of the Detection Conditions

In order to enhance sensitivity of the sensor system for Ag^+ determination, the parameters including pH, incubation time, temperature and the concentration of OPD were optimized. Firstly, the effect of pH on the fluorescence quenched efficiency was investigated in the range from pH 3.0 to 6.5. The pH value of the reaction solution has a significant influence on the response of the sensing system. OPD was easily oxidized only in the acidic environment, and so we chose citrate buffer which buffer range is pH 3.0–6.6. As shown in Fig. 3a, the maximal fluorescence quenched efficiency reached a maximum at pH 5.0. Therefore, pH 5.0 was chosen as the optimal pH for the detection of buffer solution. Fluorescence quenched efficiency was defined as $(I_0\text{-}I)/I_0$, and I_0 and I refers to the fluorescent intensity of UCNPs-OPD system in the

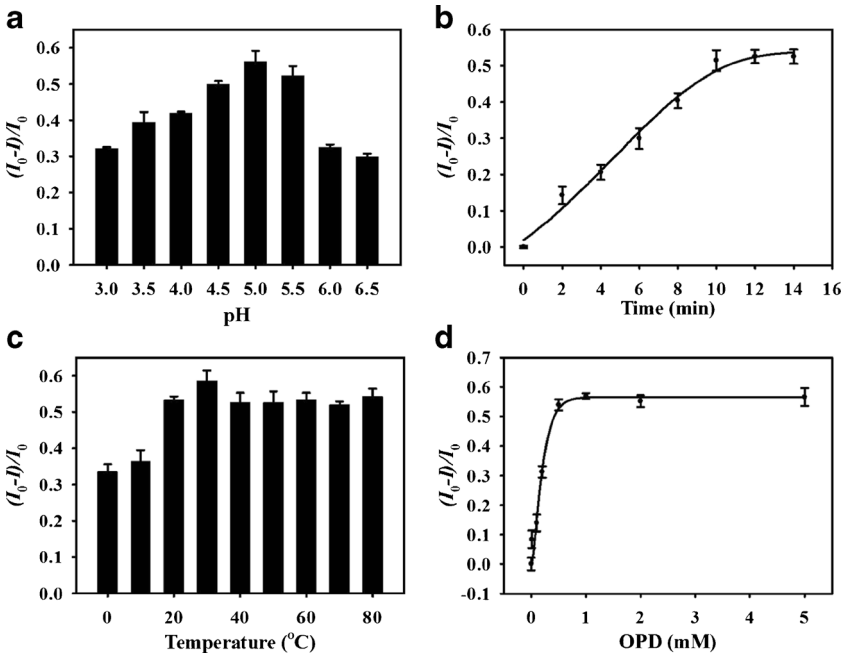

Fig. 3 Effects of pH (**a**), incubation time (**b**), temperature (**c**), and OPD concentration (**d**) on the fluorescence responses of the sensor to Ag^+ detection. I_0 and I stand for the fluorescent intensities of UCNPs in the absence and presence of Ag^+, respectively. [UCNPs]: 0.1 mg/mL. [OPD]: 1 mM. [Ag^+]: 0.1 mM

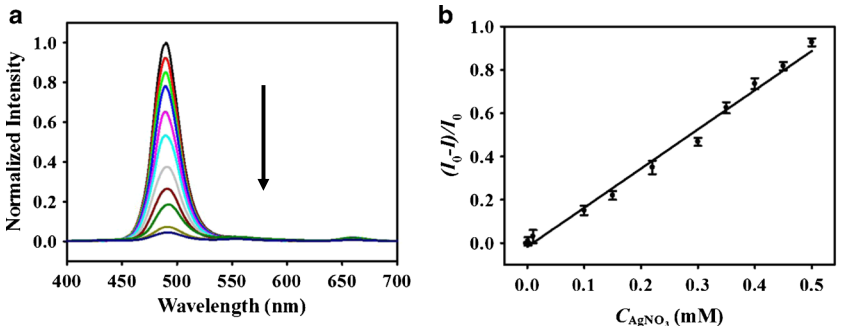

Fig. 4 (**a**) Quenching effects of UCNPs towards different concentrations of $AgNO_3$. (from top to bottom, the final concentration of $AgNO_3$ is 0, 0.001, 0.01, 0.1, 0.15, 0.22, 0.3, 0.35, 0.4, 0.45, 0.5, and 0.8 mM, respectively. (**b**) The linearity of the system towards different concentrations of $AgNO_3$

absence and presence of Ag^+, respectively. As shown in Fig. 3b, the fluorescent quenching of UCNPs-OPD system reached a maximum and sustained a stable value when the incubation time reached to 10 min. Thus, the ideal incubation time for Ag^+ detection is 10 min. We also investigated the temperature of the reaction between the UCNPs-OPD system and Ag^+. Figure 3c shows that the quenching efficiency reached a maximum when the temperature reached 30 °C. Thus, 30 °C was chosen for the following experiment. The concentrations of OPD have an influence on the sensitivity of the proposed sensing strategy for Ag^+ detection. Figure 3d display the effect of OPD concentrations of the sensing system. With the increasing concentration of OPD, the fluorescence intensity decreased rapidly and reached a stable value when the concentration of OPD was 1 mM. Hence, the concentration of OPD was selected to be 1 mM for this experiment.

Quantitative Analysis of Ag^+

Under the optimal detection conditions, the UCNPs-OPD system in the presence of various concentration of Ag^+ was investigated. As shown in Fig. 4a, the fluorescent intensity of the UCNPs-OPD mixture decreased (from top to bottom) with the increase of the Ag^+ concentration. The fluorescent spectra of the system exhibits a good linear relationship with Ag^+ in the concentration ranging from 0.0 to 0.5 mM and a linear regression equation was $F = -0.0176 + 1.8098C$ with the correlation coefficient (R^2) of 0.99 (Fig. 4b), where F refers to the measured fluorescence intensity and C refers to the concentration of Ag^+, respectively. A comparison between the method and other reported biosensors for Ag^+ determination was summarized in Table S1. The detection limit can reach as low as 33 nM, which is lower than that of the some reported methods for Ag^+ [5, 6, 22]. Our UCNPs-based fluorescent biosensor assay only needs cheap instrument and simple design, and can be performed without the presence of trained technician. In addition, our strategy has the best anti-interference performance for complex sample matrices analysis simultaneously. Thus it makes the assay with the advantages of convenience, low cost, fast, time saving and ease of operation.

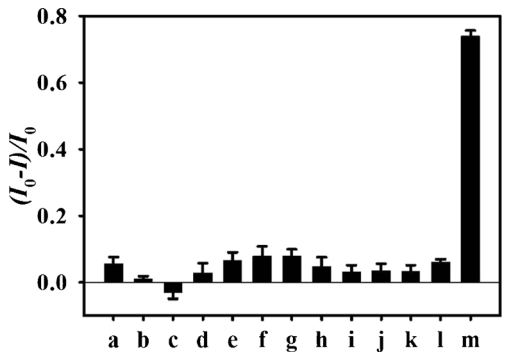

Fig. 5 Fluorescent quench of UCNPs solution mixture with Ag^+ (0.4 mM) or other substances (4 mM): (**a**) Ca^{2+}, (**b**) Cd^{2+}, (**c**) Co^{2+}, (**d**) Cu^{2+}, (**e**) Fe^{2+}, (**f**) Hg^{2+}, (**g**) Mg^{2+}, (**h**) Mn^{2+}, (**i**) Ni^{2+}, (**j**) Pb^{2+}, (**k**) Zn^{2+}, (**l**) Fe^{3+}, (**m**) Ag^+

Selectivity of the Method towards Ag^+

For determination of Ag^+ in tap water, the main interference includes other metal ions such as $CaCl_2$, $CdCl_2$, $CoCl_2$, $CuCl_2$, $FeCl_3$, $Hg(NO_3)_2$, $Mg(OAc)_2$, $MnCl_2$, $NiCl_2$, $PbCl_2$, $ZnCl_2$ and $FeCl_2$ were investigated. Typically, under optimum experimental conditions, the detection system was incubated respectively with 0.4 mM Ag^+ and 4 mM other metal ions in buffer. As is shown in Fig. 5, compared with the Ag^+ system, the existence of the other commonly seen metal ions had almost no influence on detection of Ag^+. These results demonstrated that these species did not interfere the specificity of the method for Ag^+.

Table 1 Recovery ratios of Ag^+ in tap water

Sample	Added Ag^+ (mM)	Calculate Ag^+ (mM)	Recovery(%) Ag^+	RSD(%) Ag^+
1	0.0	Not founded	98.8	4.2
	100.0	98.8		
2	150.0	155.4	103.6	3.8
3	300.0	295.2	98.4	4.9

Analysis of Ag^+ in Real Samples

In order to further investigate the potential application of the sensor in the practical samples, the assay was used to detect Ag^+ in tap water. The real samples were spiked with certain amounts of Ag^+. The assay medium and the fluorescence response of UCNPs-OPD system was detected by using the proposed strategy. The results obtained by standard addition method were listed in Table 1. As shown in Table 1, excellent quenching in the range from 98.40 % to 103.6 % was obtained. The desirable experimental results demonstrate the reliability of the proposed method for detection of Ag^+ in practical applications. In particular, low-energy NIR excitation (normally 980 nm) can overcome the interference from background fluorescence.

Conclusion

In summary, we have successfully developed a novel, convenient, sensitive, accurate and reliable fluorescent biosensor for the determination of Ag^+ based on the quenching of the fluorescence of UCNPs without complicated modification and expensive instruments. The Ag^+ concentration can be analyzed by the fluorescence of UCNPs, and the normalized fluorescence of UCNPs is quantitatively correlated to the concentration of Ag^+. Most importantly, the interference from background fluorescence and scattered light were eliminated by using the upconversion nanoparticles (UCNPs). In particular, the proposed method is successfully applied to the detection of Ag^+ in real samples. Therefore, the convenient assay provides a promising tool for developing simple, fast, low cost and sensitive sensors for Ag^+ detection.

Acknowledgments This work was supported by the National Natural Science Foundation of China (21275051, 21475043), Scientific Research Fund of Hunan Provincial Science and Technology Department and Education Department (13JJ2020, 12 A084), and Doctoral Fund of Ministry of Education of China (NO: 20134306110006).

References

1. Yang C, Sun X, Liu B (2012) Visual and trap emission spectrometric detections of Ag (I) ion with mesoporous ZnO/CdS@SiO2 core/shell nanocomposites. Anal Chim Acta 746:90–97
2. Mao K, Wu Z, Chen Y, Zhou X, Shen A, Hu J (2015) A novel biosensor based on single-layer MoS_2 nanosheets for detection of Ag^+. Talanta 132:658–663
3. Zhang Y, Jiang H, Wang X (2015) Cytidine-stabilized gold nanocluster as a fluorescence turn-on and turn-off probe for dual functional detection of Ag^+ and Hg^{2+}. Anal Chim Acta 870:1–7
4. Xu G, Wang G, Zhu Y et al (2014) Amplified and selective detection of Ag^+ ions based on electrically contacted enzymes on duplex-like DNA scaffolds. Biosens Bioelectron 59:269–275
5. Yang H, Liu X, Fei R, Hu Y (2013) Sensitive and selective detection of Ag^+ in aqueous solutions using Fe_3O_4@Au nanoparticles as smart electrochemical nanosensors. Talanta 116:548–553
6. Liu S, Tian J, Wang L, Sun X (2012) Highly sensitive and selective colorimetric detection of Ag(I) ion using 3,3′,5,5′,-tetramethylbenzidine (TMB) as an indicator. Sensors Actuators B Chem 165:44–47
7. Zhao J, Fan Q, Zhu S, Duan A, Yin Y, Li G (2013) Ultra-sensitive detection of Ag^+ ions based on Ag^+-assisted isothermal exponential degradation reaction. Biosens Bioelectron 39:183–186
8. Shi Y, Sun H, Xiang J et al (2015) I-motif-modulated fluorescence detection of silver(I) with an ultrahigh specificity. Anal Chim Acta 857:79–84
9. Chen X, Chen Y, Zhou X, Hu J (2013) Detection of Ag^+ ions and cysteine based on chelation actions between Ag + ions and guanine bases. Talanta 107:277–283
10. Chakrapani G, Mahanta PL, Murty DSR, Gomathy B (2001) Preconcentration of traces of gold, silver and palladium on activated carbon and its determination in geological samples by flame AAS after wet ashing. Talanta 53:1139–1147
11. Pu Q, Sun Q (1998) Application of 2-mercaptobenzothiazole-modified silica gel to on-line preconcentration and separation of silver for its atomic absorption spectrometric determination. Analyst 123:239–243
12. Dadfarnia S, Haji Shabani AM, Gohari M (2004) Trace enrichment and determination of silver by immobilized DDTC microcolumn and flow injection atomic absorption spectrometry. Talanta 64:682–687
13. Hosoba M, Oshita K, Katarina RK, Takayanagi T, Oshima M, Motomizu S (2009) Synthesis of novel chitosan resin possessing histidine moiety and its application to the determination of trace silver by ICP-AES coupled with triplet automated-pretreatment system. Anal Chim Acta 639:51–56
14. Krachler M, Mohl C, Emons H, Shotyk W (2002) Analytical procedures for the determination of selected trace elements in peat and plant samples by inductively coupled plasma mass spectrometry. Spectrochim Acta B At Spectrosc 57:1277–1289
15. Katarina RK, Takayanagi T, Oshima M, Motomizu S (2006) Synthesis of a chitosan-based chelating resin and its application to the selective concentration and ultratrace determination of silver in environmental water samples. Anal Chim Acta 558:246–253
16. Wygladacz K, Radu A, Xu C, Qin Y, Bakker E (2005) Fiber-optic Microsensor Array based on fluorescent bulk Optode microspheres for the trace analysis of silver ions. Anal Chem 77:4706–4712
17. Zhang X-B, Han Z-X, Fang Z-H, Shen G-L, Yu R-Q (2006) 5,10, 15-Tris (pentafluorophenyl) corrole as highly selective neutral carrier for a silver ion-sensitive electrode. Anal Chim Acta. 3/15/ 562: 210–215.
18. Achenbach JC, Nutiu R, Li Y (2005) Structure-switching allosteric deoxyribozymes. Anal Chim Acta 534:41–51
19. Mohadesi A, Taher MA (2007) Stripping voltammetric determination of silver(I) at carbon paste electrode modified with 3-amino-2-mercapto quinazolin-4(3H)-one. Talanta 71:615–619
20. Shervedani RK, Babadi MK (2006) Application of 2-mercaptobenzothiazole self-assembled monolayer on polycrystalline gold electrode as a nanosensor for determination of Ag(I). Talanta 69:741–746
21. Sung Y-M, Wu S-P (2014) Highly selective and sensitive colorimetric detection of Ag(I) using N-1-(2-mercaptoethyl)adenine functionalized gold nanoparticles. Sens Actuators B. 197:172–176.
22. Gan T-T, Zhang Y-J, Zhao N-J et al (2012) Hydrothermal synthetic mercaptopropionic acid stabled CdTe quantum dots as fluorescent probes for detection of Ag+. Spectrochim Acta A Mol Biomol Spectrosc 99:62–68
23. Lv Y, Zhu L, Liu H et al (2014) Single-fluorophore-based fluorescent probes enable dual-channel detection of Ag^+ and Hg^{2+} with high selectivity and sensitivity. Anal Chim Acta 839:74–82

24. Zhou J-C, Yang Z-L, Dong W, Tang R-J, Sun L-D, Yan C-H (2011) Bioimaging and toxicity assessments of near-infrared upconversion luminescent NaYF4:Yb,Tm nanocrystals. Biomaterials 32:9059–9067
25. Li C, Hou Z, Dai Y et al (2013) A facile fabrication of upconversion luminescent and mesoporous core-shell structured [small beta]-$NaYF_4$:Yb^{3+}, Er^{3+}@$mSiO_2$ nanocomposite spheres for anti-cancer drug delivery and cell imaging. Biomaterials Science 1: 213–223
26. Wu S, Duan N, Ma X et al (2012) Multiplexed fluorescence resonance energy transfer Aptasensor between upconversion nanoparticles and Graphene oxide for the simultaneous determination of Mycotoxins. Anal Chem 84:6263–6270
27. Liu B, Tan H, Chen Y (2013) Upconversion nanoparticle-based fluorescence resonance energy transfer assay for Cr(III) ions in urine. Anal Chim Acta 761:178–185
28. Liang L, Liu Y, Zhao X-Z (2013) Double-shell [small beta]-NaYF4: Yb^{3+}, Er^{3+}/SiO_2/TiO_2 submicroplates as a scattering and upconverting layer for efficient dye-sensitized solar cells. Chem Commun 49:3958–3960
29. Zhang W, Peng B, Tian F, Qin W, Qian X (2013) Facile preparation of well-defined hydrophilic Core–Shell upconversion nanoparticles for selective cell membrane glycan labeling and cancer cell imaging. Anal Chem 86:482–489
30. Wang X, Chen J-T, Zhu H, Chen X, Yan X-P (2013) One-step solvothermal synthesis of targetable Optomagnetic upconversion nanoparticles for in vivo bimodal imaging. Anal Chem 85:10225–10231
31. Zhang C, Yuan Y, Zhang S, Wang Y, Liu Z (2011) Biosensing platform based on fluorescence resonance energy transfer from upconverting nanocrystals to Graphene oxide. Angew Chem Int Ed 50:6851–6854
32. Yin B, Zhou W, Long Q, Li C, Zhang Y, Yao S (2014) Salt-assisted rapid transformation of $NaYF_4$:Yb^{3+},Er^{3+} nanocrystals from cubic to hexagonal. CrystEngComm 16:8348–8355
33. Liu K, Liu X, Zeng Q et al (2012) Covalently assembled NIR Nanoplatform for simultaneous fluorescence imaging and photodynamic therapy of cancer cells. ACS Nano 6:4054–4062
34. Li H, Wang L (2013) $NaYF_4$:Yb^{3+}/Er^{3+} nanoparticle-based upconversion luminescence resonance energy transfer sensor for mercury(ii) quantification. Analyst 138:1589–1595
35. Yang D, Kang X, Ma P et al (2013) Hollow structured upconversion luminescent $NaYF_4$:Yb^{3+}, Er^{3+} nanospheres for cell imaging and targeted anti-cancer drug delivery. Biomaterials 34:1601–1612
36. Xu S, Xu W, Wang Y et al (2014) NaYF4:Yb,Tm nanocrystals and TiO_2 inverse opal composite films: a novel device for upconversion enhancement and solid-based sensing of avidin. Nanoscale 6:5859–5870
37. Dong Y, Wang R, Li G, Chen C, Chi Y, Chen G (2012) Polyamine-functionalized carbon quantum dots as fluorescent probes for selective and sensitive detection of copper ions. Anal Chem 84:6220–6224
38. Badarau A, Dennison C (2011) Copper trafficking mechanism of CXXC-containing domains: insight from the pH-dependence of their Cu(I) affinities. J Am Chem Soc 33:2983–2988
39. Liu Y, Pilankatta R, Hatori Y, Lewis D, Inesi G (2010) Comparative features of copper ATPases ATP7A and ATP7B Heterologously expressed in COS-1 cells. Biochemistry 49:10006–10012
40. Shao N, Zhang Y, Cheung S et al (2005) Copper ion-selective fluorescent sensor based on the inner filter effect using a Spiropyran derivative. Anal Chem 77:7294–7303
41. Li J, Li X, Shi X et al (2013) Highly sensitive detection of Caspase-3 activities via a Nonconjugated gold nanoparticle–quantum dot pair mediated by an inner-filter effect. ACS Appl Mater Interfaces 5:9798–9802